Journal of New Technology and Materials (JNTM)
J. New Technol. Mater.
Vol. 08, N°01 (2018)102-109

OEB Univ. Publish. Co.

Predicted theoretical efficiency for new intermediate band solar cells (IBSC) based on $GaAs_{1-x}N_x$

A. Boumesjed, H. Mazari, K. Ameur, N. Benseddik, Z. Benamara and N. Benyahya

Laboratory of Applied Micro Electronics, Department of Electronics,
University Djillali Liabes of Sidi Bel Abbes, 22000 Sidi Bel Abbes, Algeria
Corresponding authors: aichaboumesjed@yahoo.fr, h_mazari2005@yahoo.fr

Received date: Jan. 20, 2018; accepted date: June 05, 2018

Abstract

Intermediate band solar cells are one type of third generation photovoltaic devices. Indeed, the increase in the power conversion efficiency is achieved through the absorption of low energy photons while preserving a large band gap that determines the open circuit voltage. The ability to absorb photons from different parts of the solar spectrum originates from the presence of an intermediate energy band located within the band gap of the material. This intermediate band, acting as a stepping stone allows the absorption of low energy photons to transfer electrons from the valence band to the conduction band by a sequential two photons absorption process.

In This work, a numerical simulation is performed using Analysis of Microelectronic and Photonic Structure (AMPS) simulator to explore the possibility of higher efficiency of intermediate band solar cell (IBSC) based on $GaAs_{1-x}N_x$ material (x=0.04). The doping density and layer thickness are investigated for optimized the performance of solar cell under solar illumination of AM1.5G. An 24.94% efficiency is determined for this new structure IBSC ($GaAs_{0.96}N_{0.01}$).

Keywords: GaAsN, Solar cell, Intermediate Band Solar Cell, Conversion efficiency;

1. Introduction

The intermediate band solar cell (IBSC) presents a somewhat simpler single-junction device alternative to multijunction devices, where the presence of an intermediate band between the conduction and valence bands allows electrons to be promoted either directly to the conduction band via a single high-energy photon, or via the intermediate band with two low-energy photons [1]. As only the populations of two lower energy transitions (valence band to IB and IB to conduction band) have to satisfy equality, the current-matching constraint, by comparison to multi-junction devices, is partially relaxed.

The key requirement for an IBSC is that the IB is isolated from the charge collecting contacts assuring that the operational voltage is determined by the largest band gap. It can also capture the solar energy from low-energy photons. The theoretical efficiency of an ideal IBSC device is predicted to approach 45% and 63% under 1 sun and maximum sunlight concentration, respectively [1].

In a conventional illuminated solar cell, the carrier populations in the conduction band (CB) and valence band (VB) can be considered to be in quasi-thermal equilibrium, meaning that thermal equilibrium exists independently within the electron population in the CB and hole population in the VB [2] but not between the two bands since an electrochemical potential difference now separates the electrons in the CB and VB giving rise to the voltage of the solar cell. In an IBSC, the voltage preservation arises from establishing a third population of carriers in the quasi-thermal IB. The occupancy of all three bands can be described using a Fermi energy, establishing three electrochemical potential differences $\mu_{1,2,3}$ as shown in figure 1 such that $\mu_1 = \mu_2+\mu_3$. Since electrical contacts are made only to the CB and VB, the overall voltage of the solar cell is given by μ_1. A limiting efficiency of 63.1% is obtained for the IBSC under the assumption of full concentration and a 6000K blackbody approximation to sunlight [1]. The correspondence between the fundamental host bandgap and the intermediate bandgap is also shown. It is clear that relatively wide bandgap host materials are required for efficient operation of an IBSC. Higher efficiencies up to 65.1% and marginally different optimal threshold energies are found when considering terrestrial solar spectrum [3]. The IBSC concept shown in figure 1 represents the optimal configuration under maximum solar concentration.

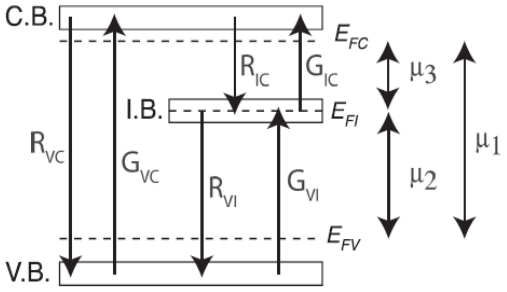

Figure 1. Schematic diagram showing the basic transitions in an IBSC [4].

2. Description of simulated solar cell

One-dimensional AMPS numerical simulation of IBSC based on the $GaAs_{0.96}N_{0.04}$ is used in this work. This code is a powerful tool to build a reasonable physical model to test the viability and numerical simulations can help to predict any changes in cell performance resulting from the modified reasonable parameters [5].

In this work, simulations were all performed under AM1.5 illumination and a temperature of 300K. The studied structure is shown in figure 2.

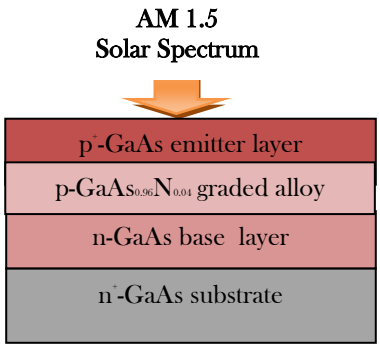

Figure 2. IBSC based on $GaAs_{0.96}N_{0.04}$.

3. Results and discussion

The optimizations of the output quantities (short-circuit current, open-circuit voltage, and conversion efficiency) will depend on the technological parameters concerning the emitter and graded alloy layer and the base in IBSC, in particular thickness and doping.

The choice of the $GaAs_{0.96}N_{0.04}$ (x = 0.04) composition for the graduated alloy is justified by the fact that currently the growth of GaAsN layers with low nitrogen concentration (experimental study) is controlled [6-8]. Practically, it is very difficult to achieve x greater than 4% without significant degradation of material quality [9]. Also, the optical parameters of this material (x = 0.04) such as: the refractive index and extinction coefficient are available in the work of A. Biswas and al [10].

The material used for our simulation consists of $GaAs_{0.96}N_{0.04}$ which has band gap energy of 1.33 eV, this value extracted from the experimental curve of the work of Ribeiro and al [11].

The electron or hole mobility is given by the following expression [12]:

$$\frac{1}{\mu(AB_{1-x}C_x)} = \frac{1-x}{\mu(AB)} + \frac{x}{\mu(AC)} + \frac{x.(1-x)}{C_\mu(AB_{1-x}C_x)} \quad (1)$$

$\mu(AB)$ and $\mu(AC)$ are the electron or hole mobility of binary AB and AC, respectively, and $\mu(AB_{1-x}C_x)$ is the alloy electron or hole mobility. Generally, the bowing of mobility C_μ is very great for III-V-N materials [12], so the last term of equation (1) tends to zero.

The absorption coefficient α is calculated from [13]:

$$\alpha = \frac{4\pi K_e}{\lambda} \quad (2)$$

Where λ is the wavelength and K_e is the extinction coefficient is as a function of the wavelength extracted from the curve of A. Biswas and al work [10].

The absorption coefficient values as a function of the wavelength for GaAs are given by [14].

In the following, the values for other parameters of GaAsN, for x = 0.04 shown in the table 1, were linearly interpolated in between the GaAs and GaN binaries.

Table 1 shows the physical parameters of GaAs, GaN, and $GaAs_{0.96}N_{0.04}$ used in simulation.

Table 1. Specific physical parameters of GaAs, GaN, and $GaAs_{0.96}N_{0.04}$.

Materials / *Physical parameters*	GaAs (ZB)	GaN (ZB)	$GaAs_{0.96}N_{0.04}$
Band gap energy, *Eg* [eV]	1.42 [15]	3.3 [18]	1.33
Electron affinity, χ [eV]	4.07 [15]	4.1 [19]	4.07
Effective density of states in the conduction band, N_c [cm^{-3}]	4.33×10^{17} [16]	1.2×10^{18} [19]	4.66×10^{17}
Effective density of states in the valence band, N_v [cm^{-3}]	1.28×10^{19} [16]	4.1×10^{19} [19]	1.39×10^{19}
Electron mobility, μ_n [$cm^2.V^{-1}.s^{-1}$]	8500 [15]	1000 [20]	6538.46
Hole mobility, μ_p [$cm^2.V^{-1}.s^{-1}$]	400 [15]	350 [21]	397.72
Relative permittivity, ε_r	12.5 [17]	9.7 [19]	12.38

3.1. Effect of the technological parameters of the emitter layer p+-GaAs

3.1.1. Effect of the doping of the emitter layer (p+-GaAs)

Figure 3 shows the variation of the photovoltaic parameters as a function of the doping of the emitter layer (p^+-GaAs). In this case, we set the parameters of IBSC based on $GaAs_{0.96}N_{0.04}$ such as the thickness of emitter layer (p^+-GaAs) and base layer (n-GaAs) of 80 nm and 2 µm, respectively. The doping of base layer (n-GaAs) and layer p-$GaAs_{0.96}N_{0.04}$ graded alloy are 1×10^{16} cm^{-3} and $1\times10^{16}$$cm^{-3}$, respectively. The thickness of layer p-$GaAs_{0.96}N_{0.04}$ graded alloy is 100 nm.

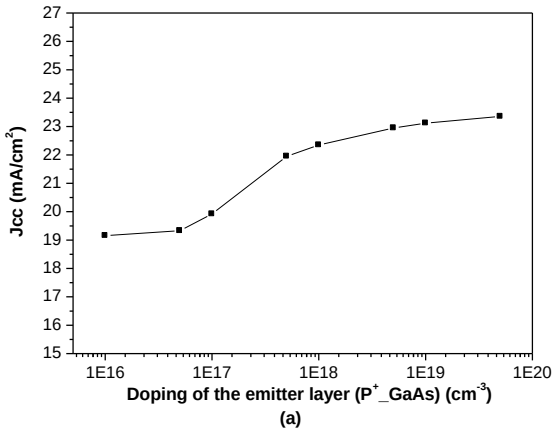

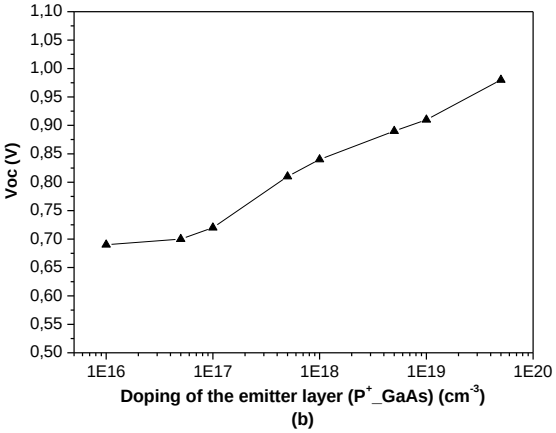

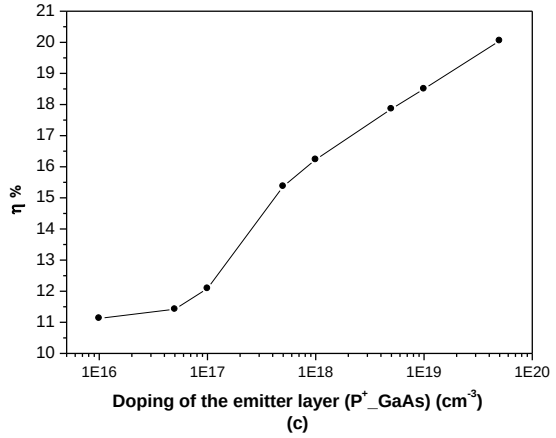

Figure 3.Variation of the photovoltaic parameters as a function of the doping of the emitter layer (p^+-GaAs).
(a)- Photocurrent I_{cc}, (b)- Open-circuit voltage V_{oc},
(c)- Conversion efficiency η.

We observe from figure 3 that the photocurrent I_{cc}, the open-circuit voltage V_{oc} and the efficiency η increase with the doping of the emitter layer.

The best conversion efficiency (η = 20.05%) is obtained for a doping of emitter layer = $5\times10^{19}cm^{-3}$.

3.1.2. Effect of thickness of the emitter layer (p^+-GaAs)

Figure 4 shows the variation of the photovoltaic parameters as a function of the thickness of the emitter layer p^+-GaAs. In this case, we set the parameters of IBSC based on $GaAs_{0.96}N_{0.04}$ such as the thickness of base layer n-GaAs and p-$GaAs_{0.96}N_{0.04}$ graded alloy of 2 µm and 100 nm, respectively. The doping of emitter layer p^+-GaAs and base layer n-GaAs are 5×10^{19} cm^{-3} and $1\times10^{16}cm^{-3}$, respectively. The doping o flayer p-$GaAs_{0.96}N_{0.04}$ graded alloy is $1\times10^{16}cm^{-3}$.

We observe from figure 4, that the photocurrent I_{cc} and the efficiency η decrease as the thickness of the emitter increases. The open-circuit voltage V_{oc} is almost constant. For small thicknesses of the emitter the photogenerated minority carriers easily reach the depletion region and can therefore contribute to the total photocurrent. But if the thickness of the emitter increases, these photocarriers recombine before reaching this zone and the photocurrent decreases.

The best conversion efficiency (η = 22.97%) is obtained for a thickness of emitter layer = 15 nm.

3.2. Effect of the technological parameters of the layer p-$GaAs_{0.96}N_{0.04}$ graded alloy

3.2.1. Effect of doping of the layer p-$GaAs_{0.96}N_{0.04}$ graded alloy

Figure 5 shows the variation of the photovoltaic parameters as a function of the doping of the p-$GaAs_{0.96}N_{0.04}$ graded alloy. In this case, we set the parameters of IBSC based on $GaAs_{0.96}N_{0.04}$ such as the thickness of emitter layer (p^+-GaAs) and base layer (n-GaAs) of 15 nm and 2 µm, respectively. The doping of emitter layer (p^+-GaAs) and base layer (n-GaAs) are 5×10^{19} cm^{-3} and 1×10^{16} cm^{-3}, respectively. The thickness of layer p-$GaAs_{0.94}N_{0.04}$ graded alloy is 2 µm.

We observe from figure 5 that the photocurrent I_{cc} and the efficiency η decrease as the doping of the p-$GaAs_{0.96}N_{0.04}$ graded alloy increases. The open-circuit voltage V_{oc} is almost constant.

The best conversion efficiency (η = 24.94%) is obtained for a doping of p-$GaAs_{0.96}N_{0.04}$ graded alloy = $1\times10^{16}cm^{-3}$.

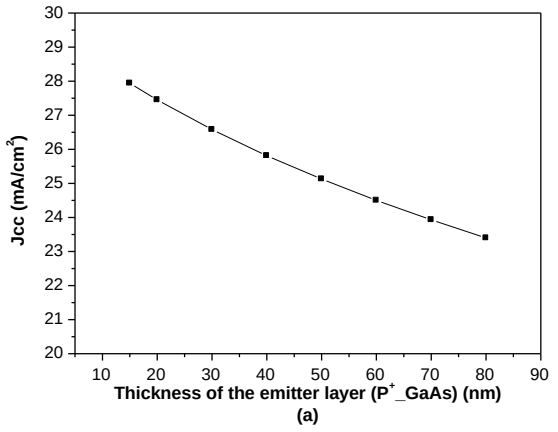

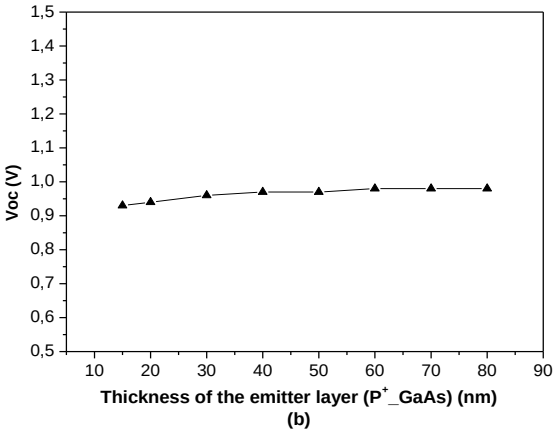

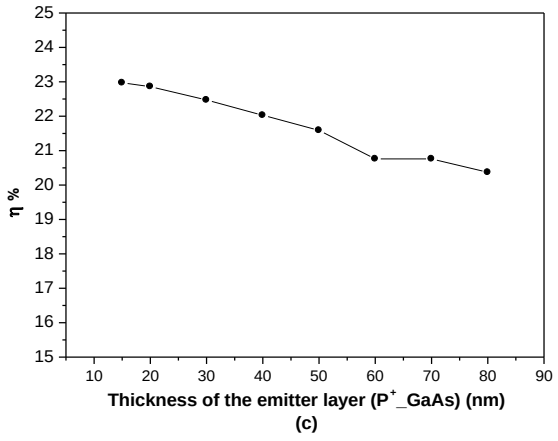

Figure 4. Variation of the photovoltaic parameters as a function of the thickness of the emitter layer (p⁺-GaAs).
(a)- Photocurrent I_{cc}, (b)- Open-circuit voltage V_{oc},
(c)- Conversion efficiency η.

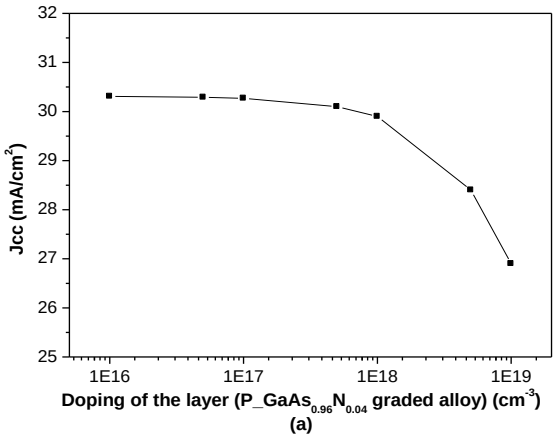

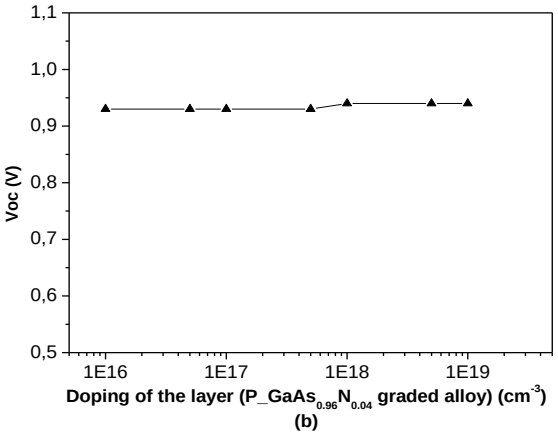

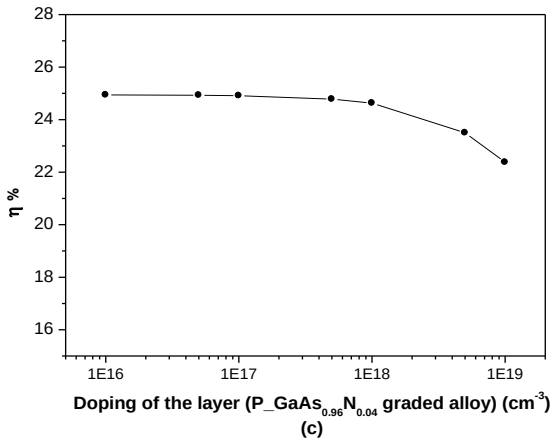

Figure 5. Variation of the photovoltaic parameters as a function of the doping of the p-$GaAs_{0.96}N_{0.04}$ graded alloy.
(a)- Photocurrent I_{cc}, (b)- Open-circuit voltage V_{oc},
(c)- Conversion efficiency η.

3.2.2. Effect of thickness of the layer p-$GaAs_{0.96}N_{0.04}$ graded alloy

Figure 6 shows the variation of the photovoltaic parameters as a function of the thickness of the layer p-$GaAs_{0.96}N_{0.04}$ graded alloy. In this case, we set the parameters of IBSC based on $GaAs_{0.96}N_{0.04}$ such as the thickness of emitter layer p^+-GaAs and base layer n-GaAs of 15 nm and 2 µm, respectively. The doping of emitter layer p^+-GaAs and base layer n-GaAs are 5×10^{19} cm^{-3} and 1×10^{16} cm^{-3}. The doping of layer p-$GaAs_{0.96}N_{0.04}$ graded alloy is 1×10^{16} cm^{-3}.

We observe from figure 6 that the photocurrent I_{cc} and the efficiency η increase with the thickness of the layer p-$GaAs_{0.96}N_{0.04}$ graded alloy. The open-circuit voltage V_{oc} remains constant.

The best conversion efficiency (η = 24.94%) is obtained for a thickness of p-$GaAs_{0.96}N_{0.04}$ graded alloy = 2 µm.

3.3. Effect of technological parameters of the base layer n-GaAs

3.3.1. Effect of the base doping (n-GaAs)

Figure 7 shows the variation of the photovoltaic parameters as a function of the doping of the base layer (n-GaAs). In this case, we set the parameters of IBSC based on $GaAs_{0.96}N_{0.04}$ such as the thickness of emitter layer (p^+-GaAs) and base layer (n-GaAs) of 15 nm and 2 µm, respectively. The doping of emitter layer (p^+-GaAs) and layer p-$GaAs_{0.96}N_{0.04}$ graded alloy are 5×10^{19} cm^{-3} and 1×10^{16} cm^{-3}, respectively. The thickness of layer p-$GaAs_{0.96}N_{0.04}$ graded alloy is 2 µm.

We note from figure 7 a no variation is observed at the change in the doping of the base layer.

3.3.2. Effect of thickness of the base layer (n-GaAs)

Figure 8 shows the variation of the photovoltaic parameters as a function of the thickness of the base layer. In this case, we set the parameters of IBSC based on $GaAs_{0.96}N_{0.04}$ such as the thickness of emitter layer p^+-GaAs and layer p-$GaAs_{0.96}N_{0.04}$ graded alloy of 15 nm and 2 µm, respectively. The doping of emitter layer p^+-GaAs and base layer n-GaAs are 5×10^{19} cm^{-3} and 1×10^{16} cm^{-3}. The doping of layer p-$GaAs_{0.96}N_{0.04}$ graded alloy is 1×10^{16} cm^{-3}.

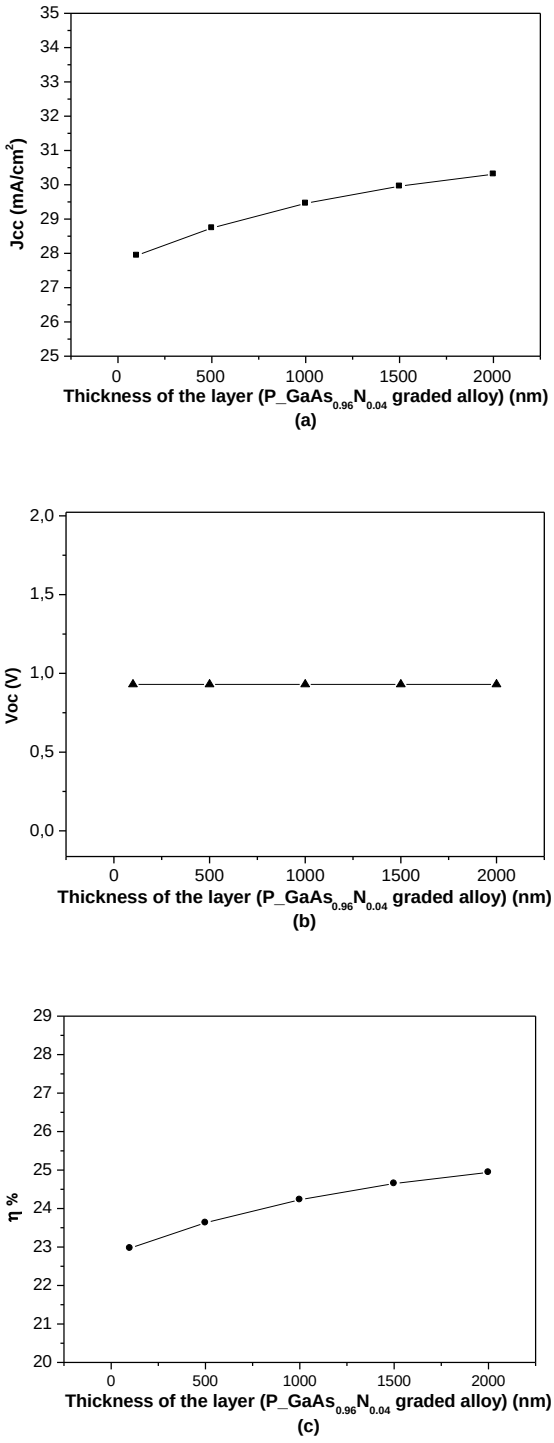

Figure 6. Variation of the photovoltaic parameters as a function of the thickness of the p-$GaAs_{0.96}N_{0.04}$ graded alloy. (a)- Photocurrent I_{cc}, (b)-Open-circuit voltage V_{oc}, (c)- Conversion efficiency η.

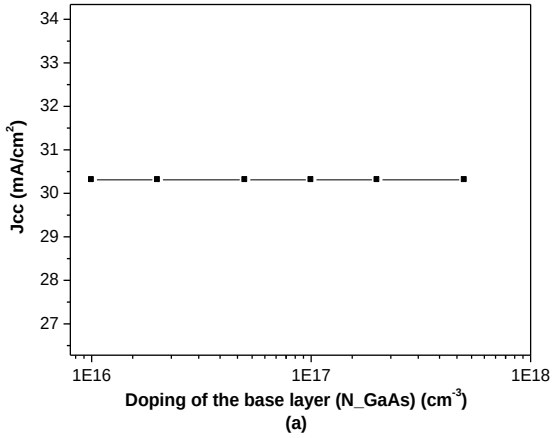

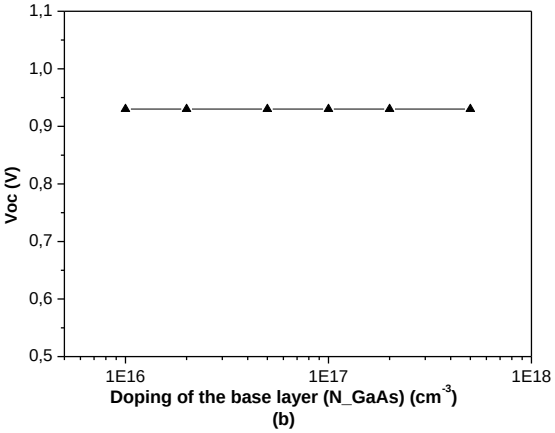

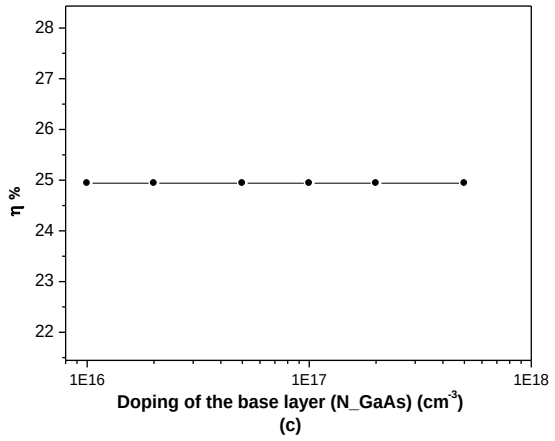

Figure 7. Variation of the photovoltaic parameters as a function of the doping of the base layer (n-GaAs).
(a)- Photocurrent I_{cc}, (b)- Open-circuit voltage V_{oc},
(c)- Conversion efficiency η.

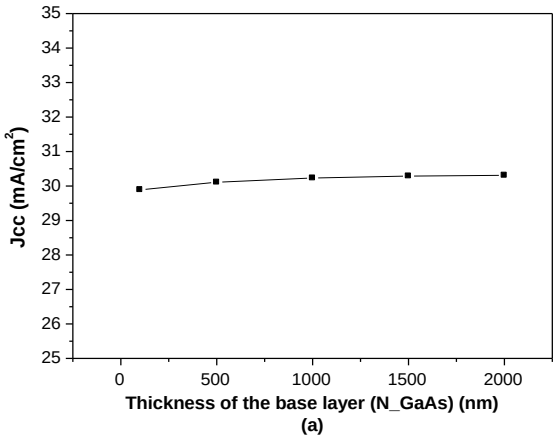

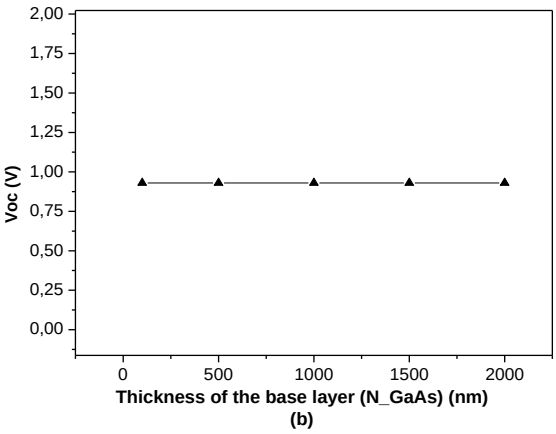

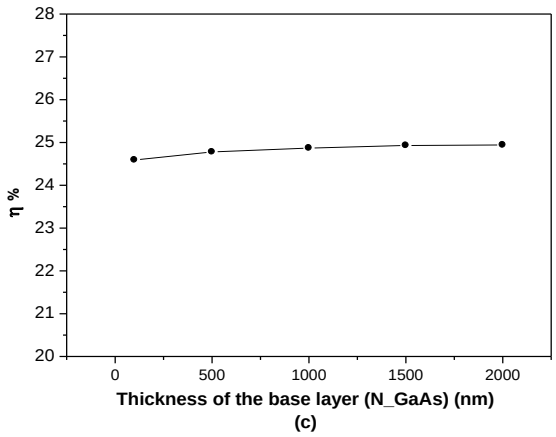

Figure 8. Variation of the photovoltaic parameters as a function of the thickness of the base layer (n-GaAs).
(a)- Photocurrent I_{cc}, (b)- Open-circuit voltage V_{oc},
(c)- Conversion efficiency η.

We observe from figure 8 that the photocurrent I_{cc} and the efficiency η are almost constant, the open-circuit voltage V_{oc} remains constant.

We observed that the IBSC based on $GaAs_{0.96}N_{0.04}$ gives high conversion efficiency that, when we choose the optimization we have done for the necessary parameters to the simulation.

We can summarize the optimized parameters for this structure in the following table.

Table 2. Optimized parameters of IBSC $GaAs_{0.96}N_{0.04}$.

Parameters	Values
Doping of the emitter layer (p^+-GaAs) (cm^{-3})	5×10^{19}
Thickness of the emitter layer (nm)	15
Doping of the p-$GaAs_{0.96}N_{0.04}$ graded alloy (cm^{-3})	1×10^{16}
Thickness of the layer p-$GaAs_{0.96}N_{0.04}$ graded alloy (µm)	2
Doping of the base layer (cm^{-3})	1×10^{16}
Thickness of the base layer (µm)	2

The simulated J-V curve of the optimized cell is shown in figure 9. We observe that the output final characteristics are satisfactory with Jsc = 30.31 mA/cm², Voc = 0.93 V and η = 24.94%.

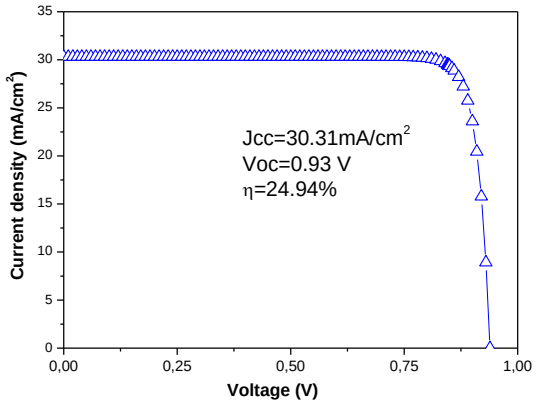

Figure 9. J-V characteristics for the optimized solar cell.

4. Conclusion

The work presented in this paper concerns the study of intermediate band solar cell IBSC based on the $GaAs_{0.96}N_{0.04}$. The main objective is to optimize the electrical characteristic of the proposed photovoltaic cell and subsequently its output parameters.

The device design studied here appears as promising, the key parameters success of this approach are:

- It is necessary to minimize the thickness of the base (p^+GaAs) and to increase doping.
- It is necessary to increase the thickness of the layer (Intermediate band) p-$GaAs_{0.96}N_{0.04}$ graded alloy and decrease the doping.

Finally, we obtained a maximum conversion efficiency of 24.94% in this preliminary study for IBSC based on $GaAs_{0.96}N_{0.04}$.

References

[1] A. Luque and A. Martí, Phys. Rev. Lett.78 (1997) 5014-5017.
[2] P. Würfel, Sol. Energy Mater. Sol. Cells 38, 23 (1995).
[3] S. P. Brenner, M. Y. Levy, and C. B. Honsberg, Appl. Phys. Lett. 92,171110 (2008).
[4] Y. Okada, N. J. Ekins-Daukes, T. Kita and al., Appl. Phys. Lett. 105, 011120 (2014); 10.1063/1.4889805.
[5] "AMPS Manual", The Electronic Materials and Processing Research Laboratory at the Pennsylvania State University, University Park, Pennsylvania, Pennsylvania State University, (2007).
[6] F. Hassen, Z. Zaaboub, M. Bouhlel, M. Naffouti, H. Maaref, N.M. Garni, Thin Solid Films 594 (2015) 168–171
[7] X. Z. Chen, D. H. Zhang, Y. J. Jin, J. H. Li, J. H. Teng, N. Yakovlev, Journal of Crystal Growth 362 (2013) 197–201
[8] R. Carron, "Dilute-NitrideLow-Dimensional Nanostructures Formed on Non-PlanarSubstrates", Thèse, École Polytechnique Fédéralede Lausanne, France (2013).
[9] A. Vallejo Luce, "Engineering Dilute Nitride Semiconductor Alloys for Intermediate Band Solar Cells", thesis, University of California, Berkeley, USA (2015).
[10] A. Biswas , B. S. Yadav , D. Bhattacharyya , N. K. Sahoo , S. S. Major , R. S. Srinivasa, Journal of Non-Crystalline Solids 357, (2011)3293–3300
[11] A. Ribeiro, F. J. Ribeiro, A. S. Martins, Solid State Communications 186 (2014) 50–55.
[12] R. Quay, « Gallium Nitride electronics », Springer Series in Materials Science, Vol. 96, 24-25 (2008).
[13] J. D. Majumdar, I. Manna, "Laser-Assisted Fabrication of Materials", Springer-Verlag Berlin Heidelbrg (2013).
[14] D. A. Clugston, P. A. Basore, PC1D version 5: 32-bit solar cell modelling on personal computers. Conference Record of the 26th IEEE Photovoltaic Specialists Conference, (1997) 207–210.
[15] M. Levinstein, S. Rumyantsev and M. Shur, Handbook Series on Semiconductor Parameters" vol. 1,2 , World Scientific, London, (1996), (1999).

[16] B. Boittiaux, Cours d'électronique: Les composants semiconducteurs, 2ème édition, TEC & DOC (EDITIONS) (1995).
[17] S. W. Koch, Microscopic Theory of Semiconductors: Quantum Kinetics, Confinement and Lasers, 212, World Scientific, (1995).
[18] I. Vurgaftman, J. R. Meyer, and L. R. Ram-Mohan, J. Appl. Phys., 89, 5815-5875 (2001).
[19] https://fr.scribd.com/document/98540290/Gan-Band-Str
[20] J. G. Kim, A. C. Frenkel, H. Liu and R.M. Park, Appl. Phys. Lett., 65, 91-93 (1994).
[21] J. R. L. Fernandez, V. A. Chitta, E. Abramof, A. Ferreira da Silva, J. R. Leite, A. Tabata, D. J. As, T. Frey, D. Schikora, and L. Lischka, (in: GaN and Related Alloys - 1999. Symposium (Materials Research Society Symposium Proceedings Vol.595); Warrendale, PA, USA: Mater. Res. Soc, (2000).